Detection of collective modes in unconventional superconductors using tunneling spectroscopy

Patrick A. Lee[1] and Jacob F. Steiner[2]

[1]*Department of Physics, Massachusetts Institute of Technology, Cambridge, Massachusetts 02139, USA*

[2]*Department of Physics and Institute for Quantum Information and Matter, California Institute of Technology, Pasadena, California 91125, USA*

(Received 5 July 2023; accepted 16 October 2023; published 3 November 2023)

We propose using tunneling spectroscopy with a superconducting electrode to probe the collective modes of unconventional superconductors. The modes are predicted to appear as peaks in dI/dV at voltages given by $eV = \omega_i/2$ where ω_i denotes the mode frequencies. This may prove to be a powerful tool to investigate the pairing symmetry of unconventional superconductors. The peaks associated with the collective modes appear at fourth order in the single-particle tunneling-matrix element. At the same fourth order, multiple Andreev reflection (MAR) leads to peaks at voltage equal to the energy gaps, which, in BCS superconductors, coincides with the expected position of the amplitude (Higgs) mode. The peaks stemming from the collective modes of unconventional superconductors do not suffer from this coincidence. For scanning tunneling microscopes, we estimate that the magnitude of the collective mode contribution is smaller than the MAR contribution by the ratio of the energy gap to the Fermi energy. Moreover, there is no access to the mode dispersion. Conversely, for planar tunnel junctions the collective mode peak is expected to dominate over the MAR peak, and the mode dispersion can be measured. We discuss systems where the search for such collective modes is promising.

DOI: 10.1103/PhysRevB.108.174503

I. INTRODUCTION

In the past three decades, many examples of unconventional superconductors (SCs) have been discovered. Many of these have multiple order parameters, either due to pairing in several disconnected Fermi surfaces, or due to pairing that is intrinsically multicomponent. In the latter case, the order parameters may be members of a particular irreducible representation, prime examples being MgB_2 [1] and the iron-based superconductors [2]. Alternatively, they are of mixed symmetry due to the breaking of lattice or time-reversal symmetry. While there are numerous examples of mixed symmetry pairing, very often it is difficult to identify the precise order parameter symmetry in these materials. In an interesting recent paper Poniatowski *et al.* [3] pointed out that, since these systems exhibit collective modes beyond the familiar phase and amplitude (Higgs) modes, the detection of these modes may serve as signature of the order parameter symmetry. They investigated several examples and showed that commonly these modes lie below the quasiparticle gap 2Δ and hence form well-defined excitations. Some of these collective modes are analogs of the Leggett mode [4], or of the "clapping" mode, familiar from the He^3 literature [5,6]. While progress in the detection of such modes has been made using nonlinear optical spectroscopy [7], they are often charge neutral and thus evade detection using conventional tools. Motivated by this, we study the question of whether the collective modes of unconventional superconductors may be detected using tunneling spectroscopy. We investigate point contact tunneling such as scanning tunneling microscopy (STM) as well as planar tunneling and compare their respective advantages and disadvantages. We will also discuss examples where such experiments may be feasible.

This paper is structured as follows. In Sec. II we demonstrate within linear response theory how collective modes of the pairing give rise to features in the tunneling current between two SCs. In Sec. III we discuss processes that give rise to features in the tunneling current at the same order in perturbation theory which are commonly observed, namely the Josephson peak and multiple Andreev reflections (MAR). In Sec. IV we present a microscopic treatment of the current due to collective modes, which includes the possibility of multi-component order parameters. In Sec. V we discuss the magnitude of the features in the collective mode relative to the Josephson peak and the leading order MAR contribution. We proceed in Sec. VI by applying our results to several experimentally relevant multi-component SCs, highlighting examples where it is promising to look for the current due to collective modes. Finally, in we conclude Sec. VII with a discussion of the experimental challenges associated with measuring the current due to collective modes.

II. COLLECTIVE MODES IN THE TUNNELING SPECTRUM

The idea of using tunneling to detect pair fluctuations goes back to the seminal papers by Ferrell [8] and Scalapino [9]. They were interested in pair fluctuations above the critical temperature T_c, and pointed out that the pair fluctuations appear in linear response to an external pairing order parameter, just like magnetization fluctuations appear as the linear susceptibility to an external magnetic field. More specifically, they considered a tunnel junction with voltage bias V between two SCs L (left) and R (right) with different $T_{c,j}$ and energy gaps Δ_j, $j \in \{L, R\}$, where the left SC is assumed to have a higher T_c. The pair-tunneling Hamiltonian is ob-

tained by expanding the Josephson energy E_J of a junction with area A to linear order in Δ_R, which is then replaced by the pair-destruction operator $\hat{\Delta}_R(\boldsymbol{r}) = |g_0|\,\psi_{R,\downarrow}(\boldsymbol{r})\psi_{R,\uparrow}(\boldsymbol{r})$, g_0 being the BCS coupling. This gives the coupling Hamiltonian

$$H_{\text{pair}} = \int d\boldsymbol{r}\, C e^{-i2eVt}\,\hat{\Delta}_R(\boldsymbol{r}) + \text{H.c.}, \tag{1}$$

which oscillates at the Josephson frequency $2eV$ (setting $\hbar = 1$). Here, we defined the coupling strength $C = \partial(E_J/A)/\partial\Delta_R$ as well as the Josephson energy $E_J = (g/4\pi)\Delta_R K(\sqrt{1-\Delta_R^2/\Delta_L^2})$ in terms of the elliptic function K. Moreover, we introduced the dimensionless conductance $g = (h/e^2)/R_N$, where R_N is the junction resistance in the normal state [10]. In the limit $\Delta_L \gg \Delta_R$, $E_J = (g/2\pi)\Delta_R \ln(4|\Delta_L/\Delta_R|)$, and we recover the expressions given in Ref. [9]. Standard linear response theory gives the current as

$$I_{\text{pair}}(V,H) = 4eC^2A\,\text{Im}\,\chi_R(\boldsymbol{q} = 2\boldsymbol{q}_H, \omega = 2eV), \tag{2}$$

where $\chi_R(\boldsymbol{q},\omega)$ is the Fourier transform of the pair susceptibility

$$\chi_R(\boldsymbol{r},t) = -i\langle[\hat{\Delta}_R(\boldsymbol{r},t),\hat{\Delta}_R(0)^\dagger]\rangle\theta(t), \tag{3}$$

and $2\boldsymbol{q}_H$ is the pair momentum induced by a magnetic field H parallel to the junction [9]. (We have assumed that R is a two-dimensional SC. Otherwise, the current will depend on the thickness of R provided it is less than the coherence length; cf. Ref. [9].)

The pair fluctuations were successfully measured very close to the transition temperature $T_{c,R}$ [11]. In principle, there is no reason why the same arguments cannot be applied to low temperatures. In that case, the collective mode dispersion corresponds to poles in $\chi_R(\boldsymbol{q},\omega)$ and should manifest as peaks in the tunneling current. In fact, this has been proposed as a way to measure the Higgs mode [12]. In practice, peaks corresponding to putative collective modes have never been observed in tunneling experiments. A purpose of this paper is to explain this absence, and to point out the conditions under which such observations may become successful in the future.

III. JOSEPHSON PEAK AND MULTIPLE ANDREEV REFLECTIONS

We begin by noting that the current I_{pair} is proportional to g^2 and thus fourth order in the tunneling-matrix element. We first consider the STM case and consider other terms to the same order in the tunneling current. STM spectra exhibit subgap structures stemming from processes commonly known as multiple Andreev reflection (MAR) [13,15]. They may be calculated in an expansion in powers of the tunneling-matrix element [14]. At fourth order, the first set of MAR peaks appears at $eV = \Delta_L$ and Δ_R in dI/dV. They correspond to processes where a pair tunnels across the junction and gains an energy $2eV$. For $2eV > 2\Delta_R$ this energy can go into exciting a pair of quasiparticles on the R side. This gives rise to a step threshold in the current $I(V)$ and consequently a peak in dI/dV at $eV = \Delta_R$. A similar argument produces a step at Δ_L. MAR peaks are commonly seen in STM when the tip is brought close to the surface, increasing g [13,15]. The ratio of the lowest-order MAR peak in dI/dV to the conductance above the coherence peak threshold is simply of order g (see Fig. 1). We note that g of order 0.01 or even unity can be achieved [13,17]. Nevertheless, collective modes such as the Higgs mode have not been reported in STM experiments. One reason lies in the fact that, in conventional SC, the phase mode is pushed up to the plasma frequency and the only remaining collective mode is the Higgs mode which has energy $2\Delta_R$. This gives rise to a peak at $eV = \Delta_R$ which happens to coincide with the lowest-order MAR peak. Furthermore, as shown below, in STM the magnitude of the collective mode contribution is reduced from the MAR magnitude by a factor Δ_R/E_F where E_F is the Fermi energy of the R SC. This reduction stems from point tunneling: in this case, the current involves a convolution over the momentum of the mode. The latter disperses rapidly on the scale of the inverse coherence length ξ^{-1}, giving rise to this suppression. We conclude that the collective mode may be visible in STM only for strongly correlated materials where the factor Δ_R/E_F is not too small.

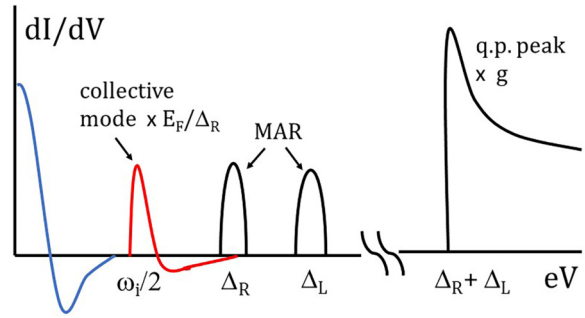

FIG. 1. Schematic drawing of the STM tunneling conductance dI/dV with a SC tip (with energy gap Δ_L) showing the expected subgap features up to fourth order in the tunneling amplitude. The standard quasiparticle peak starting at $\Delta_R + \Delta_L$ has been reduced by $g = (h/e^2)/R_N$, the dimensionless normal-state conductance. Below this energy we find the multiple Andreev reflection (MAR) peaks at Δ_R and Δ_L which overlap the respective amplitude (Higgs) modes. Shown in red is the contribution from a collective mode for an unconventional SC on the R side at frequency ω_i. It consists of a peak at $eV = \omega_i/2$ and a tail toward higher voltage. Its height has been multiplied by E_F/Δ_R. Shown in blue is the Josephson current that has been broadened by dissipation. The line shape is given by Eq. (4) for $kT_0 \gg E_J$ which is the typical situation [15] and is much narrower in the opposite limit [16]. The collective mode is the new feature discussed in this paper.

Another contribution to the same order in g^2 commonly seen in STM is the Josephson current broadened by thermal noise. Thermal fluctuations dephase the junction and convert the Josephson current from a delta function to a peak structure at low but finite bias. The theory has been given by Ivanchenko and Zilberman [18]. The result depends on the relative size of the Josephson energy E_J of the junction to the noise temperature k_BT_0. (Note that T_0 is in general different from and larger than the sample temperature T.) In the limit $E_J \ll k_BT_0$ the current is given by

$$I_J(V) = e\frac{E_J^2}{k_BT_0}\frac{2eV\Gamma_0}{(2eV)^2+\Gamma_0^2}, \tag{4}$$

where the width is given by $\Gamma_0 = k_BT_0R_0(2e)^2$ with the dissipation parametrized by an effective resistance R_0. More

specifically, the external circuit is modeled by a series resistance R_0 (not to be confused with the normal-state junction resistance R_N) which gives rise to voltage fluctuations across the junction characterized by $\langle \delta V(t)\delta V(t')\rangle = 2k_BT_0R_0\delta(t-t')$. Note that in Eq. (4) the maximum current is proportional to E_J^2/T_0 which is proportional to g^2. In fact, STM data are usually in this limit: the line shape predicted by Eq. (4) is often seen as a peak in dI/dV whose height is comparable to and scales in the same way as the MAR peak at $eV = \Delta_R$ with changing tip height [15]. On the other hand, planar junctions are in the opposite limit $E_J \gg k_BT_0$ because E_J scales with the area. In this case, the peak is very narrow and steep [16]. A useful physical picture is that of an overdamped particle moving in a tilted "washboard potential." In the limit $E_J \ll k_BT_0$ thermal fluctuations lead to rapid jumps over the washboard barrier and give rise to phase slips, resulting in Eq. (4).

In the case of the Josephson current, the voltage bias is small and the washboard is relatively flat. In the case of the collective mode we are in a large-voltage regime where the phase is running rapidly down the washboard and subject to weak modulation due to E_J. In this case the phase across the junction is given to a good approximation by $\theta(t) \approx 2e[V_{\rm ext}t + \int_0^t dt'\delta V(t')]$. Hence, the fluctuating part of the phase correlation is given by $\langle(\delta\theta(t) - \delta\theta(0))^2\rangle = (2e)^2 2k_BT_0R_0t$. Inserting this into Eq. (3), we find that the effect of thermal noise is to introduce an additional Lorentzian convolution to the response function, with a width given by Γ_0. Similar arguments show that the width of the MAR peak is also given by Γ_0 (see Appendix B). Thus, the minimal width of all the subgap structures shown in Fig. 1 is set by the width of the Josephson peak in Eq. (4) which can be readily measured. It follows that a condition for the visibility of the collective mode is simply that its width given by Γ_0 is not so large that it will overlap other features such as the Josephson peak or the MAR peak. Note that the width of the collective mode and the MAR peak are the same whether k_BT_0 is large or small compared with E_J. Only the Josephson peak is affected by this condition.

IV. MICROSCOPIC TREATMENT OF THE CURRENT DUE TO COLLECTIVE MODES

Next, we turn to a microscopic treatment of the problem, including the multicomponent SCs mentioned in the introduction. We will derive an extension of the pair-tunneling Hamiltonian Eq. (1) by calculating the in-gap current to fourth order in $t_{k,p}$, following earlier work by Takayama [19]. The voltage drop across the junction can be absorbed into a time-dependent tunneling-matrix element $t_{k,p}e^{ieVt}$, rendering the SC leads at equilibrium. This allows a treatment within the conventional Matsubara formalism, and the more elaborate Keldysh treatment [14] is not necessary. The in-gap current due to collective modes of the R SC is then given by the diagram Fig. 2(c). Details of the calculation are presented in Appendix A. Below, we discuss the main results.

In the STM case, tunneling occurs at a single point and does not resolve the momentum of the pair response function as in Eq. (2). Instead, the current involves an integral over the momentum $\boldsymbol{q}$:

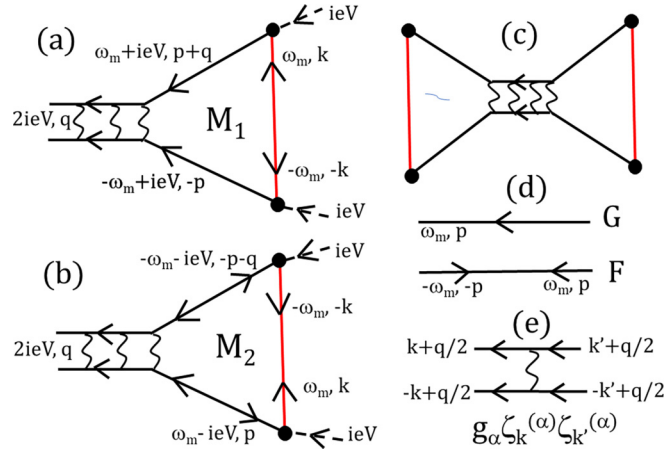

FIG. 2. Diagrams that contribute to the STM tunneling current to fourth order in the tunneling-matrix element $t_{k,p}$ represented by the solid dot. The diagram that couples to the collective mode is shown in (c) where the double line represents the pair propagator of the R SC which is related to the pair susceptibility $\chi_{\alpha,\beta}(\boldsymbol{q}, \omega = 2eV)$ by analytic continuation. (a) and (b) show the two diagrams M_1 and M_2 that contribute to the triangle on the right side of (c). Two similar diagrams contribute to the left triangle related to the right triangle by complex conjugation. The anomalous Green function of the L SC is shown in red. In (a) the R SC Green function is the regular G while in (b) it is the anomalous F function. The latter is shown in (d). Note that frequency and momentum reverse sign on opposite ends of F. (e) shows the BCS coupling in separable form for each channel α.

$$I_{\rm STM}(V) = 4e\sum_{\alpha,\beta}\int d\boldsymbol{q}\, M_\alpha^*(\boldsymbol{q}, V)M_\beta(\boldsymbol{q}, V)\,{\rm Im}\,\chi_{\alpha,\beta} \times (\boldsymbol{q}, \omega = 2eV). \tag{5}$$

Here, we have introduced multiple pairing order parameters $\Delta_{\boldsymbol{k}}^{(\alpha)}$ for the R SC. We will drop the R label from now on. The label α may refer to pairing in different bands, or to members of a irreducible representation, or to superposition of different pairing symmetries when time-reversal or crystalline symmetry is spontaneously broken. Following Ref. [3], we assume a separable form for the attractive interaction $U_{\boldsymbol{k},\boldsymbol{k}'} = -\sum_\alpha g_\alpha \zeta_{\boldsymbol{k}}^{(\alpha)}\zeta_{\boldsymbol{k}'}^{(\alpha)}$, where the $\zeta_{\boldsymbol{k}}^{(\alpha)}$ are orthonormal form factors and the g_α are the coupling constants in the corresponding channel. We neglect the dependence on $\boldsymbol{q}$, the center-of-mass momentum of the Cooper pair. This vertex is shown in Fig. 2(e). The pair-destruction operator is generalized to $\hat\Delta_{\boldsymbol{k}}^{(\alpha)}(\boldsymbol{q}) = g_\alpha\sum_{\boldsymbol{k}}\zeta_{\boldsymbol{k}}^{(\alpha)}c_{-\boldsymbol{k},\downarrow}^{(\alpha)}c_{\boldsymbol{k}+\boldsymbol{q},\uparrow}^{(\alpha)}$. For simplicity of notation, we assume singlet pairing, but the calculation can be straightforwardly extended to general pairing symmetry. The pair susceptibility can be generalized from Eq. (3) in a natural way as

$$\chi_{\alpha,\beta}(\boldsymbol{q}, t) = -i\langle\big[\hat\Delta_{\boldsymbol{k}}^{(\alpha)}(\boldsymbol{q}, t),\, \hat\Delta_{\boldsymbol{k}}^{(\beta)}(\boldsymbol{q}, 0)^\dagger\big]\rangle\theta(t). \tag{6}$$

The matrix element $M_\alpha(\boldsymbol{q}, V)$ is given by the sum of M_1 and M_2, which are defined by the two triangle diagrams shown in

Figs. 2(a) and 2(b), respectively. It is

$$M_\alpha(\boldsymbol{q},V)=T\sum_{\omega_m}\int d\boldsymbol{k}\,d\boldsymbol{p}\,|\tilde{t}|^2\zeta_{\boldsymbol{p}}^{(\alpha)}F_L(\boldsymbol{k},\omega_m)\times\left[G_R^{(\alpha)}(\boldsymbol{p}+\boldsymbol{q},\omega_m+ieV)G_R^{(\alpha)}(-\boldsymbol{p},-\omega_m+ieV)-F_R^{(\alpha)}(\boldsymbol{p}+\boldsymbol{q},\omega_m+ieV)F_R^{(\alpha)}(-\boldsymbol{p},-\omega_m+ieV)\right]. \tag{7}$$

Here, as appropriate for STM tunneling, we have neglected the momentum dependence of the tunneling-matrix element $t_{\boldsymbol{k},\boldsymbol{p}}$, replacing it by $\tilde{t}$. We have further used the fact that the anomalous electron Green function satisfies $F_{\downarrow\uparrow}(\boldsymbol{k},\omega_m)=-F_{\uparrow\downarrow}(\boldsymbol{k},\omega_m)$ which accounts for the negative sign in the second term. Note that one factor of $\zeta_{\boldsymbol{k}}^{(\alpha)}$ enters the matrix element in Eq. (7) and one factor enters the pair susceptibility in Eq. (5). It is easy to see that the left triangle in Fig. 2(c) is the complex conjugate of the right triangle. The product $\zeta_{\boldsymbol{p}}^{(\alpha)}F_L(\boldsymbol{k},\omega_m)$ in Eq. (7) determines which components of the pair fluctuation can be probed. For example, if L is a conventional s-wave SC, only collective modes with a component α corresponding to s wave will couple, as we shall illustrate by an example below.

Based on the form Eq. (5), we suggest a nonlocal generalization of the pair-tunneling Hamiltonian,

$$\tilde{H}_{\rm pair}=\sum_\alpha\int d\boldsymbol{r}'\,\tilde{C}_\alpha(\boldsymbol{r}-\boldsymbol{r}',V)e^{-i2eVt}\,\hat{\Delta}_R^{(\alpha)}(\boldsymbol{r}')+\text{H.c.}, \tag{8}$$

for STM tunneling at position $\boldsymbol{r}$. [Integration over $\boldsymbol{r}$ in Eq. (8) gives the generalization of Eq. (1) for planar junctions.] It is clear that linear response based on Eq. (8) leads to Eq. (5) if we identify the Fourier transform of $\tilde{C}_\alpha(\boldsymbol{r},V)$ with $M_\alpha(\boldsymbol{q},V)$. As shown in Appendix A, M has a smooth V dependence which can usually be ignored. More importantly, Eq. (5) involves a convolution in momentum space between the pair susceptibility and the product of the matrix element. We find that $M_\alpha(\boldsymbol{q},V)$ goes to a constant for small q and falls off with q on a scale given by the inverse of the coherence length ξ_R when $\Delta_L\gtrsim\Delta_R$ (see Appendix A for details). The physical origin of the nonlocality in Eq. (8) and the convolution over $\boldsymbol{q}$ in Eq. (5) is that the Cooper pair is injected from the L SC one electron at a time by the single-particle tunneling-matrix element. Consequently quasiparticles exist virtually over a distance of order ξ_R before recombining to form a Cooper pair on the R SC. We note that for the single order parameter case the simple pair-tunneling Hamiltonian Eq. (1) can be readily derived from Eq. (8). Focusing on the planar case, in the absence of a magnetic field, and for $V\ll\Delta_R$, it is $\tilde{C}\simeq M(\boldsymbol{q}=0,V=0)/A=\partial(E_J/A)/\partial\Delta_R$ (see Appendix A), fully consistent with Eq. (1).

V. VISIBILITY

Next, we estimate the magnitude of the collective mode contribution to the current. For simplicity we discuss the single order parameter case. In this case, the inverse pair propagator generically takes the form $\chi^{-1}(\boldsymbol{q},\omega_n)=N(0)[1+(\omega_n^2+b_iv_F^2q^2)/(a_i\Delta^2)]$, where a_i and b_i are numbers of order unity [3]. The zeros of this function give the collective mode dispersion $\omega_i(q)$. The pair susceptibility thus takes the form

$$\text{Im}\,\chi(\boldsymbol{q},\omega)=\frac{1}{N(0)}\frac{\pi\omega_{i0}^2}{2\omega_i(\boldsymbol{q})}\delta(\omega-\omega_i(\boldsymbol{q})), \tag{9}$$

where $\omega_i^2(\boldsymbol{q})=\omega_{i0}^2+b_iv_F^2q^2$ and $\omega_{i0}=\sqrt{a_i}\Delta$. Note that the dispersion is very steep: $\omega_i(\boldsymbol{q})$ roughly doubles in value when q is of order the inverse of the coherence length $\xi=v_F/\pi\Delta$. In planar junctions this form leads to delta functions in the current $I(V)$ at $2eV=\omega_i(\boldsymbol{q})$. Thus, planar junction tunneling allows access to the dispersion of the mode. This is not the case which requires an additional integration over $\boldsymbol{q}$. Instead of a delta function, the $I(V)$ now features a step at $2eV=\omega_{i0}$ followed by a smooth drop-off on a scale set by $M(\boldsymbol{q},V)$. The step function gives rise to a delta function in dI/dV,

$$\frac{dI_{\rm STM}}{dV}=e^2\frac{8\pi^2a_i\Delta^2}{N(0)b_iv_F^2}|M(0,V)|^2\delta(2eV-\omega_{i0}), \tag{10}$$

which is followed by a negative tail toward larger voltages as sketched in Fig. 1. To estimate M in Eq. (10), it suffices to consider its $V=0$ limit. Focusing on a symmetric junction $\Delta_R=\Delta_L=\Delta$, it is $M=\partial E_J/\partial\Delta=g/8$ [10]. With this, we may compare the peak in dI/dV due to the collective mode to the step in the MAR current which is given by $eg^2\Delta$ [14]. (See also Appendix B.) Using $N(0)=m/2\pi$ and $E_F=mv_F^2/2$ we find the relative magnitude of the collective mode and MAR steps to be approximately Δ/E_F as stated earlier. For conventional SCs this ratio is very small which makes the detection of the collective mode infeasible. Nonetheless, there are now examples of strongly correlated SCs where this ratio is not very small. It is worthwhile to look for the collective mode contribution in STM in such systems.

The situation is more promising for planar junctions. (See Appendix A for details.) It is useful to consider the ratio of the collective mode current $I_{\rm planar}$ to the current in the normal state at $eV=2\Delta_R$ which is given by $I_N=2\Delta/(eR_N)$. For simplicity, we again consider the symmetric case $\Delta_R=\Delta_L=\Delta$. We find the ratio

$$\frac{I_{\rm planar}}{I_N}=\frac{\pi^3}{32}\frac{a_ig}{Ak_F^2}\frac{\Delta E_F}{\omega_{i0}}\frac{\Gamma}{(2eV-\omega_{i0})^2+\Gamma^2}. \tag{11}$$

Here, we have replaced the delta function in Eq. (9) by a Lorentzian with width Γ which is given by Γ_0 plus other sources of broadening such as inhomogeneity. A similar ratio for the planar MAR current is obtained in Appendix B, where it is found to have parametrically the same prefactor up to numerical constants, but with the Lorentzian in Eq. (11) replaced by $(eV/\Delta)[(eV)^2-\Delta^2]^{-1/2}$. The latter should also be broadened by voltage noise and inhomogeneity. Since this form is less singular than the Lorentzian, the collective mode contribution should dominate over the MAR peak in planar junctions, in contrast to the situation in STM. More precisely, with the same broadening Γ, the peak currents due to the collective mode and the MAR have a ratio of $\sqrt{\Delta/\Gamma}$ which is greater than 1.

We now address the size of the signal from the collective mode contribution given by Eq. (11). We interpret Ak_F^2 as the number of tunneling channels in a planar junction and use the Landauer formula to define the ratio $\mathcal{T}_{\rm eff}=g/(Ak_F^2)$ as the effective tunneling probability per channel. $\mathcal{T}_{\rm eff}$ gives

the intrinsic transparency of a tunnel junction and is generally a very small number. Conversely, the peak value of the Lorentzian is $1/\Gamma_i$, and the ratio E_F/Γ_i is a very large number. For a typical planar junction, $\mathcal{T}_{\rm eff}$ is so small that the product is still too small to be observable for reasonable Γ_i. This may be the reason why neither MAR nor collective modes have been observed in planar junctions. However, as we shall see, the numbers are not too far off, and there may be reasons for optimism. To see this we estimate that for the typical oxide tunnel barrier used in Ref. [11], the transparency is $\mathcal{T}_{\rm eff} \approx 10^{-8}$ (assuming $A \sim 100^2$ nm^2, $k_F \sim 1$ Å^{-1}, and $R_N \sim 2\ \Omega$). In this experiment a fluctuating pair-tunneling peak with width of about 1 μeV was readily observed. We conclude that a collective mode with width of order 1 μeV should be observable in a conventional oxide planar junction, because the signal in Eq. (11) is proportional to the ratio $\mathcal{T}_{\rm eff}/\Gamma_i$. The minimal contribution to the width comes from voltage fluctuations and the corresponding Γ_0 can be made very small [16]. In practice, in many of the strongly correlated SCs of interest, such as cuprates or iron-based SCs, local inhomogeneity may lead to significant broadening of the collective mode in planar junctions. Their detection may require higher tunneling transparency $\mathcal{T}_{\rm eff}$ and possibly smaller area junctions. The latter requirement will reduce the current, making the experiment more challenging.

Apart from the larger signal compared with STM, we note that the current itself is predicted to show a narrow peak, so that the dI/dV signal is the derivative of a Lorentzian which has a distinctive line shape with a large negative part. Furthermore, the planar junction has the advantage that the dispersion of the collective mode may be probed by applying an in-plane magnetic field. These distinctive features will provide strong evidence that a collective mode is being observed.

VI. PROMISING EXPERIMENTAL PLATFORMS

Now, we discuss several multicomponent examples where the collective modes may be detected in $I(V)$ or dI/dV as sharp peaks. We note that generalization of Eqs. (10) and (11) to the case of multiple order parameters is straightforward. Indeed, one may assume that the pair susceptibility takes the form of a weighted sum of delta functions, $\mathrm{Im}\,\chi_{\alpha,\beta}(\boldsymbol{q},\omega) = \sum_i w^i_{\alpha,\beta}(\boldsymbol{q})\delta(\omega-\omega_i(\boldsymbol{q}))$. This translates directly into a sum of peaks at $2eV = \omega_{i0}$ and weighted by $w^i_{\alpha,\beta}$ in the dI/dV [$I(V)$] for STM [planar] tunneling. We expect the magnitude estimates, which were obtained above in the single order parameter case, to apply also in the more general case. For simplicity, we assume that the SC being probed is inversion symmetric. If the L SC is conventional, only s-wave Cooper pairs can be injected from the L electrode and only the α-components corresponding to s-wave pairing survive. Consider first multiband SCs, where s-wave pairing occurs in two different Fermi surfaces $\alpha = 1, 2$, as, e.g., in MgB_2 and in iron-based superconductors. In the latter case the two s-wave components are out of phase, referred to as $s_\pm$ state. We expect a collective mode (the Leggett mode) corresponding to the out-of-phase oscillation of the two order parameters $\Delta^{(1)}$ and $\Delta^{(2)}$. This mode will manifest as a pole in $\chi_{1,2}$. The Leggett mode has been observed by Raman scattering in MgB_2 at a relatively high energy of 9.2 meV which lies between the two doubled energy gaps [20]. Hence, this mode is damped, but it is nonetheless interesting to search for this peak within tunneling spectroscopy. We note that MgB_2 planar tunneling junctions have been successfully fabricated [21]. For the Fe-based SCs, the situation is not so clear. We note that recently an observation of the Leggett mode was reported in single-layer $NbSe_2$ in an experiment using a normal STM tip [22]. Here, the Leggett mode is interpreted as giving an excitation above the gap at energy $\Delta + \omega_i$. Interestingly, the experiment found that $\omega_i/2 \approx 0.7\Delta$ which places the peak well inside the gap and well below the MAR structure. Note that $NbSe_2$ features a small ratio of Δ/E_F so that the STM signal of the Leggett mode is expected to be very small, but perhaps a planar junction experiment can be attempted.

As a second application we consider the case of a time-reversal-breaking SC, more specifically of the type $s+id$, i.e., an admixture of s- and d-wave pairing. This case is treated in detail in Ref. [3] and here we only summarize the salient features. The important point is that the presence of the s-wave component allows us to couple to novel collective modes such as clapping modes. We define the s- and d-wave order parameter components as $(\Delta^{(0)}, \Delta^{(2)}) = (\eta_0, -i\eta_2)\Delta_0 e^{i\theta}$, where θ is the overall pair phase, and η_0 and η_2 are real numbers satisfying $\eta_0^2 + \eta_2^2 = 1$. It is convenient to introduce $\Delta^\pm = \Delta^{(0)}/\eta_0 \pm \Delta^{(2)}/(i\eta_2)$. The saddle-point solution occurs at $\Delta^+ = \Delta_0$ and $\Delta^- = 0$. Expanding around the saddle point we find the coordinates of the collective modes as

$$\Delta^+(\boldsymbol{r},t) = e^{i\theta}[\Delta_0 + h(\boldsymbol{r},t)], \tag{12}$$

$$\Delta^-(\boldsymbol{r},t) = e^{i\theta}[a(\boldsymbol{r},t) + ib(\boldsymbol{r},t)]. \tag{13}$$

Here, h denotes the amplitude or Higgs mode, while a and b denote two new modes which are generalizations of the clapping mode in $p+ip$ SCs. Poniatowski *et al.* [3] show that these modes lie at approximately $\sqrt{2}\Delta_0$. We will now show that they appear in the s-wave pair fluctuation channel in Eq. (10). To this end, we expand

$$\Delta^{(0)}(\boldsymbol{r},t) = e^{i\theta}[\eta_0\Delta_0 + \tilde{\Delta}^{(0)}(\boldsymbol{r},t)]. \tag{14}$$

It is easy to see that the fluctuating part is given by

$$\tilde{\Delta}^{(0)}(\boldsymbol{r},t) = \eta_0[h(\boldsymbol{r},t) + a(\boldsymbol{r},t) + ib(\boldsymbol{r},t)]. \tag{15}$$

Hence, all three modes will appear in the $\alpha = 0$ pair fluctuation component in Eq. (10). In particular, the generalized clapping modes will show up as peaks in the vicinity of $eV = \Delta_0/\sqrt{2}$, well separated from the MAR peak at Δ_0. This is shown schematically in Fig. 1. In the iron-based SC $Ba_{1-x}K_xFe_2As_2$, a time-reversal-breaking SC state appears for x between 0.7 and 0.8 and is suspected to be an $s+id$ SC [23]. This is an excellent candidate to search for these collective modes.

We consider a third example of triplet pairing where the time-reversal-breaking state may be of the $p+ip$ or $p+if$ type. UTe_2 may be an example [24]. This rather complicated structure preserves inversion in the bulk, but it is possible, indeed likely, that the top layer breaks inversion due to some local structural relaxation. In this case the s-wave pair injected by the L SC is admixed with the p- and f-wave order parameter in the first layer of the R SC, and the matrix element M_α in Eq. (5) is nonzero for non-s-wave components. In this way,

collective modes may couple to the current. Indeed, a recent STM experiment using a Nb tip found a subgap peak near the expected energy gap for UTe_2 and a peak in dI/dV near zero voltage suggestive of a broadened Josephson current [24]. The latter observation points to an admixture of s-wave pairing in the top layer, as we need. Unfortunately, the ratio Δ/E_F may be too small for STM to observe the collective mode in this system.

VII. DISCUSSION

We end by discussing the feasibility of probing collective modes of unconventional SC using either planar or STM tunnel junctions. It is generally considered difficult to make planar tunnel junctions in these systems, but with modern fabrication techniques it may be possible to create nanoscale tunnel junctions with high transparency that are free of pinholes. Another approach may involve stacks of van der Waals materials such as transition metal dichalcogenides (TMDs). A variety of insulating TMDs may be used to create monolayer barriers between SC layers. In cuprates, a single layer of insulating parent state may be used as tunneling barrier [25]. On the STM front, it has been demonstrated that it is possible to pick up a piece of layered SC with an STM tip, which then serves as the SC electrode [26]. This holds promise for the present application: e.g., a cuprate SC tip would allow the collective modes of systems with d-wave [27] or $d+id$ pairing symmetry to be probed. As noted above, the detection of collective modes in STM relies on a relatively large ratio of Δ/E_F. Recently, a range of strongly correlated SCs have been discovered, which represent promising candidates for the present proposal. Notable examples are twisted bilayer and trilayer graphene, where the ratio is so large that the BEC limit may be reached [28]. Another example is the iron-based topological SCs, which have very small Fermi energy [17]. An example that is not well understood is the superconductivity observed in YPtBi which involves doping of a quadratic touching band with a very small Fermi energy and a short coherence length [29]. We conclude that, while they are challenging, tunneling experiments probing the signatures of the collective modes in unconventional SCs are within reach.

ACKNOWLEDGMENTS

We thank Shuqiu Wang and Seamus Davis for sharing their data on UTe_2 which stimulated this investigation. We thank Nicholas Poniatowski, Leonid Glazman, and Iliya Esin for helpful discussions. P.A.L. acknowledges support by DOE (USA) office of Basic Sciences Grant No. DE-FG02-03ER46076. J.F.S. acknowledges support by the Air Force Office of Scientific Research under Award No. FA9550-22-1-0339.

APPENDIX A: DERIVATION OF TUNNELING CURRENT DUE TO COLLECTIVE MODES

We model the junction by the single-electron tunneling Hamiltonian

$$H_{\rm tun}=\sum_{\boldsymbol{k},\boldsymbol{p},\sigma} t_{\boldsymbol{k},\boldsymbol{p}} e^{ieVt} c^\dagger_{L,\boldsymbol{k},\sigma} c_{R,\boldsymbol{p},\sigma} + \text{H.c.}, \tag{A1}$$

where we have included the voltage V across the junction through time-dependent tunneling. In this framework, one may assume the electrons of both sides to be in equilibrium and standard Matsubara diagrammatic techniques may be applied. The DC current is given by averaging the current operator related to $H_{\rm tun}$ over time,

$$I=\frac{1}{\beta}\int_0^\infty d\tau I(\tau) = -\frac{2e}{\beta}\sum_{kp\sigma}\text{Im}\int_0^\infty d\tau \langle T_\tau t_{\boldsymbol{k},\boldsymbol{p}} e^{i(ieV)\tau} c^\dagger_{Lk\sigma} \times (\tau) c_{Rp\sigma}(\tau) U(\beta)\rangle, \tag{A2}$$

where we defined the imaginary-time evolution operator

$$U(\beta)=T_\tau \exp\left[-\int_0^\beta d\tau' H_{\rm tun}(\tau')\right]. \tag{A3}$$

(See Appendix B for a more careful treatment of the time-dependent factor in imaginary time.) We can now expand Eq. (A2) to fourth order in $t_{\boldsymbol{k},\boldsymbol{p}}$ and proceed with the usual decoupling into products of Green functions. We are interested in diagrams that involve the imaginary-time ordered pair propagator for the R SC,

$$\chi_{\alpha,\beta}(\boldsymbol{q},\tau)=-\langle T_\tau[\hat\Delta^{(\alpha)}_{\boldsymbol{k}}(\boldsymbol{q},\tau)\,\hat\Delta^{(\beta)}_{\boldsymbol{k}}(\boldsymbol{q},0)^\dagger]\rangle. \tag{A4}$$

Upon Fourier transform and analytic continuation, $\chi_{\alpha,\beta}(\boldsymbol{q}, i\omega_n\to\omega+i\eta)$, η positive infinitesimal, becomes the retarded pair susceptibility defined in Eq. (6). The relevant diagrams are shown in Fig. 2(c). They consist of the propagator connected to a triangular graph on each side. The sides of the triangle that connect to χ must refer to the R SC, which means the remaining side refers to the L SC. Furthermore, this side must couple to the anomalous propagator F_L because we want to inject a pair from L to R. There are two versions of the triangles, depending on whether the L Green function is the normal G or the anomalous F. We call the ones on the right of the pair propagator M_1 and M_2. It is easy to see that the ones on the left are the respective complex conjugates. In this way, we arrive at Eq. (7) where $M=M_1+M_2$. After analytic continuation, we obtain Eq. (5). Note that the voltage eV is injected at each tunneling vertex and is passed directly to the pair propagator. This has the important consequence that the voltage gives a direct measure of the collective mode frequency via $2eV=\omega_i$.

1. Collective mode: STM junction

The momentum label on the triangles depends on the nature of the tunnel junction. We first discuss the STM or point contact tunneling case. The corresponding diagrams are shown in Figs. 2(a) and 2(b). To simplify notation, we consider a single s-wave component and suppress the α label. The tunneling occurs at a single point, which means that $t_{\boldsymbol{k},\boldsymbol{p}}$ is independent of momentum and can be set to a constant $\tilde t$. In contrast to frequency, momentum is not conserved at the vertex for tunneling at a point. The integration over k for the L SC can be done separately, which simply gives the anomalous Green function at $\boldsymbol{r}=0$, i.e., $F_L(\boldsymbol{r}=0,\omega_n)=\pi N_L(0)\Delta_L/\sqrt{\omega_m^2+\Delta_L^2}$, where $N(0)$ is the density of states at the Fermi level. Furthermore, a finite momentum q is passed on to the propagator, which needs to be integrated over. This

gives rise to the integral over $\boldsymbol{q}$ shown in Eq. (4). This is the main difference between STM and planar tunneling, as shall be discussed below.

The full expression for $M(\boldsymbol{q}, V)$ requires numerical integration. Here we consider some simple limits. First we set $\boldsymbol{q} = 0$ and then consider the expansion to quadratic order in $\boldsymbol{q}$. Equation (7) becomes

$$\begin{aligned} M(\boldsymbol{q}=0, V=0) &= T\sum_m \tilde{t}^2 F_L(\boldsymbol{r}=0, \omega_m) \\ &\times \int d\boldsymbol{p}\,[G_R(\omega_m, \boldsymbol{p})G_R(-\omega_m, -\boldsymbol{p}) \\ &- F_R(\omega_m, \boldsymbol{p})F_R(-\omega_m, -\boldsymbol{p})] \qquad \text{(A5)} \\ &= T\sum_m \tilde{t}^2 \frac{\Delta_L}{\sqrt{\omega_m^2+\Delta_L^2}} N_L(0)N_R(0) \\ &\times \int d\xi_p \left[\left(\frac{i\omega_m+\xi_p}{\omega_m^2+E_p^2}\right)\left(\frac{-i\omega_m+\xi_p}{\omega_m^2+E_p^2}\right)\right. \\ &\times \left. -\frac{\Delta_R^2}{(\omega_m^2+E_p^2)^2}\right], \qquad \text{(A6)} \end{aligned}$$

where $E_p = \sqrt{\Delta^2+\xi_p^2}$ and $\xi_p = \epsilon(\boldsymbol{p}) - \mu$. We have set $V = 0$ in this expression because its dependence on V is expected to be smooth for the following reason. As seen from the diagrams in Fig. 2, the effect of V is to shift ω_m to $\omega_m + ieV$ and $\omega_m - ieV$ in the two normal Green functions G. The sum over ω_m in Eq. (A5) can be converted to an integral over the real variable $\omega_m \to \omega$ in the $T \to 0$ limit. It is clear that adding an imaginary part will affect the integral in a smooth way.

The factor in square brackets in Eq. (A5) can be written as

$$\begin{aligned} &\frac{1}{\omega_m^2+\xi_p^2+\Delta_R^2} - \frac{2\Delta_R}{\left(\omega_m^2+\xi_p^2+\Delta_R^2\right)^2} \\ &= \frac{d}{d\Delta_R}\left[\frac{\Delta_R}{\omega_m^2+\xi_p^2+\Delta_R^2}\right]. \qquad \text{(A7)} \end{aligned}$$

On the other hand, the Josephson energy is given by [10]

$$\begin{aligned} E_J &= T\sum_m \tilde{t}^2 \int d\boldsymbol{k}d\boldsymbol{p}\, F_L(\omega_m, \boldsymbol{k})F_R(\omega_m, \boldsymbol{p}) \\ &= T\sum_m \tilde{t}^2 N_L(0)N_R(0)\int d\xi_p \frac{\Delta_L}{\sqrt{\omega_m^2+\Delta_L^2}}\frac{\Delta_R}{\omega_m^2+\xi_p^2+\Delta_R^2}. \qquad \text{(A8)} \end{aligned}$$

Hence, we find that

$$M(\boldsymbol{q}=0, V=0) = \frac{\partial E_J}{\partial \Delta_R} \qquad \text{(A9)}$$

as quoted in the text.

Next we calculate the leading q^2 term in $M(\boldsymbol{q}, V)$. We expand $\xi_{p+q} \approx \xi_p + v_F q\cos\theta$ where θ is the angle between $\boldsymbol{p}$ and $\boldsymbol{q}$. We keep only the linear in q term in this expansion. This amounts to assuming a constant Fermi velocity v_F. After a straightforward but laborious calculation, we arrive at

$$\begin{aligned} &M(\boldsymbol{q}, V=0) - M(\boldsymbol{q}=0, V=0) \\ &\approx -v_F^2 q^2 \frac{\pi}{4}\tilde{t}^2 N_L(0)N_R(0)\int \frac{d\omega}{2\pi}\frac{\Delta_L}{\sqrt{\omega^2+\Delta_L^2}}\frac{\Delta_R^2-\omega^2}{\left(\Delta_R^2+\omega^2\right)^{5/2}} \qquad \text{(A10)} \\ &= -q^2\xi_R^2\frac{\pi^2}{8}\tilde{t}^2 N_L(0)N_R(0) f(y=\Delta_L/\Delta_R), \qquad \text{(A11)} \end{aligned}$$

where we defined the BCS coherence length of the R SC $\xi_R = v_F/\pi\Delta_R$, as well as the dimensionless function

$$f(y) = y\int dw \frac{1}{\sqrt{w^2+y^2}}\frac{1-w^2}{(1+w^2)^{5/2}}. \qquad \text{(A12)}$$

For $y \gg 1$, $f \to 2/3$, while for $y \ll 1$ it behaves as $f \sim y\ln 1/y$. At $\Delta_L = \Delta_R$, $f(1) = \pi/4$. Thus, for $\Delta_L \gg \Delta_R$ and $\Delta_L \sim \Delta_R$, $M(\boldsymbol{q}, V=0)$ decreases with q on the scale of the inverse of the coherence length ξ_R. The physical picture is that the injected quasiparticle pair can travel a distance ξ_R in the R SC before forming a Cooper pair. In the $\Delta_L \ll \Delta_R$ limit the scale depends on Δ_L as well.

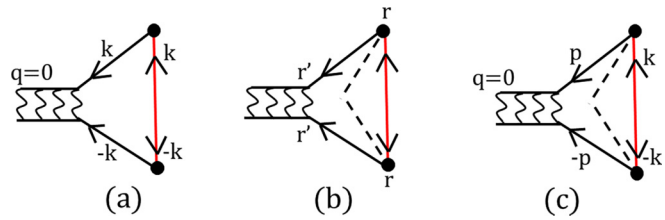

FIG. 3. Diagrams that contribute to M_1 in planar tunnel junctions. (a) Momentum parallel to the plane is conserved. (b), (c) Diffusive case. Dashed line represents averaging over the random tunneling-matrix elements. (b) is in position space. Note that the averaging forces both ends of the red line to be at the same $\boldsymbol{r}$. (c) The momentum-space version of (b) obtained by Fourier transform.

2. Collective mode: Planar junction

We now turn to the case of a planar tunnel junction. We consider two tunneling models. First, we assume that momentum parallel to the plane is conserved during the tunneling process. The momentum labels in the triangle graph are shown in Fig. 3(a). Note the difference from the STM case shown in Fig. 2. Now there is only one momentum integration. Importantly, the pair propagator carries momentum $q = 0$. This will be changed to q_H in the presence of a parallel magnetic field [9]. In contrast to the STM case, there is no convolution over $\boldsymbol{q}$. We thus recover the prediction from linear response to the pair-tunneling Hamiltonian Eq. (1). Second, we consider diffusive scattering at the junction interface. We follow Takayama [19] and assume local tunneling of the form

$$H_{\text{local tun}} = \int d\boldsymbol{r}\,\hat{t}(\boldsymbol{r})\sum_\sigma \psi_{L,\sigma}^\dagger(\boldsymbol{r})\psi_{R,\sigma}(\boldsymbol{r}) + \text{H.c.}, \qquad \text{(A13)}$$

where $\boldsymbol{r}$ is the spatial coordinate in the plane, and $\hat{t}$ is a random variable such that $\langle\hat{t}(\boldsymbol{r})\hat{t}(\boldsymbol{r}')\rangle = t_0^2\delta(\boldsymbol{r}-\boldsymbol{r}')$. This model has the desirable feature that the current, when computed to fourth order in t_0, scales correctly with the junction area. A

more realistic model would have a nonzero average $\langle \hat{t}(\boldsymbol{r})\rangle$. This latter part conserves parallel momentum and thus may be included by simply adding the diagrams of Figs. 3(a) and 3(c). In Fig. 3(b) we show the triangle diagram in real space where the dashed line represents averaging over the random variable. Upon Fourier transform we obtain the diagram in momentum space as shown in Fig. 3(c). The momentum transfer to the pair propagator is zero in this case. In a parallel magnetic field, momentum $\boldsymbol{q}_H$ is injected at the tunneling vertices, leading to $\boldsymbol{q}_H$ dependence of M and excitation of the collective mode at $2\boldsymbol{q}_H$. We conclude that in both cases, the planar tunneling case can be described by a pair-tunneling Hamiltonian which is analogous to Eq. (1), except that C should be replaced by a slowly varying function of V which is nonlocal in space. Indeed, this function is readily obtained from its Fourier transform $\tilde{C}(\boldsymbol{q}, V) = M(\boldsymbol{q}, V)$, as described in the main text below Eq. (8).

APPENDIX B: CALCULATION OF LEADING MAR SUBGAP STRUCTURES

In this section we employ the Matsubara method to treat the leading MAR structure which is fourth order in the tunneling-matrix element. The equivalent calculation was done by Cuevas *et al.* [14] for the STM case using the Keldysh technique. We first present results for the planar tunneling case, including also finite-temperature effects. We were not able to find this case treated in the literature, and we find the Matsubara method to be less laborious than the Keldysh method, even though some subtlety is involved.

As noted in the text, the voltage drop across the junction can be absorbed into a time-dependent tunneling-matrix element $t_{\boldsymbol{k},\boldsymbol{p}}e^{ieVt}$. After this step the SCs in the leads are at equilibrium so that conventional Matsubara method can be used. This was done in calculating the matrix element M that couples to the collective mode in the last section. The proper procedure was given by Tsuzuki [30] and used by Takayama [19]. The idea is to introduce $\Omega_n = 2\pi nT$, where n is a positive integer, and replace $t_{\boldsymbol{k},\boldsymbol{p}}e^{ieVt}$ by $t_{\boldsymbol{k},\boldsymbol{p}}e^{i\Omega_n\tau}$, where $\tau = it$. In this way the evolution in τ is unitary. At the end of the calculation, after internal Matsubara frequencies have been summed, we replace $i\Omega_n$ with eV. In a slight departure from Tsuzuki, we keep the adiabatic turning on term $e^{\eta t}$ as $e^{-i\eta\tau}$ so that $i\Omega_n \to eV + i\eta$. We will see that failure to follow this procedure will result in erroneous thermal factors. This subtlety did not arise in the calculation of the matrix element M in the previous section which involves only virtual excitations of quasiparticles. In contrast MAR involves the real excitation of quasiparticles and their thermal occupation appears in a crucial way.

1. MAR: Planar junction

To illustrate this point, we give some details for the case of planar junctions with diffusive scattering using the random tunneling model described in the last section [19]. A representative diagram for the current that shows the flow of momentum and frequency is shown in Fig. 4(a). There are other diagrams where each solid line can be either G or F functions. In other words, the diagram should be viewed as the trace of the matrix product of four Green functions in Nambu space. In addition, the dashed line representing averaging over random tunneling-matrix elements can connect the ends of the solid lines on the top and bottom instead of left and right as shown in Fig. 4(a). However, its contribution can be shown to be less singular. Here, we show the evaluation of this particular diagram which we label by i. The sum over $\boldsymbol{k}$ and $\boldsymbol{k}'$ converts the anomalous Green function F_L to the local form, and we have a single sum over $\boldsymbol{p}$. We write the contribution of this diagram to the MAR current for the diffusive planar junction as

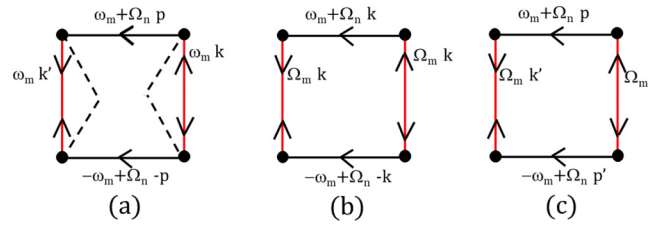

FIG. 4. Representative diagrams that contribute to the MAR currents. (a) Planar junction, diffusive case. Dashed line represents averaging over the random tunneling-matrix elements. (b) Planar junction, clean case. Momentum parallel to the plane is conserved resulting in a single momentum integral over k. (c) STM case. The tunneling-matrix element represented by the solid dots add or remove Matsubara frequency Ω_n which is analytically continued to $\Omega_n \to eV + i\eta$ after the sum over ω_m is performed. In addition to the diagrams shown, each solid line can be either G or F functions.

$$I^{\rm MAR}_{{\rm planar},i} = 4e|t_0|^4 {\rm Im}\, J_i(i\Omega_n \to eV + i\eta), \tag{B1}$$

where

$$J_i(i\Omega_n) = T\sum_m |F_L(x=0,\omega_m)|^2 A \int d\boldsymbol{p}\,[G_R(\omega_m+\Omega_n,\boldsymbol{p}) \times G_R(-\omega_m+\Omega_n,-\boldsymbol{p})] \tag{B2}$$

$$= T\sum_m \frac{\pi^2\Delta_L^2}{\omega_m^2+\Delta_L^2} N_L^2(0) N_R(0) A \int d\xi_{\boldsymbol{p}} \times \left[\frac{i\omega_m + i\Omega_n + \xi_{\boldsymbol{p}}}{(i\omega_m+i\Omega_n)^2 - E_{\boldsymbol{p}}^2}\right]\left[\frac{-i\omega_m + i\Omega_n + \xi_{\boldsymbol{p}}}{(-i\omega_m+i\Omega_n)^2 - E_{\boldsymbol{p}}^2}\right]. \tag{B3}$$

Here A is the junction area. The sum over m is done in the standard way by extending $i\omega_m$ to the complex z and converting $\int d\xi$ to $\int dE\, E/\sqrt{E^2-\Delta^2}$ where $E = \sqrt{\xi^2+\Delta^2}$. There are 6 poles z_i in Eq. (B2). The sum over n leads to a sum over the product of the residues of these poles and $n_F(z_i)$ where n_F is the Fermi function. For $eV > 0$ the important poles are at $z_3 = i\Omega_n - E$ and $z_2 = -z_3$. The Fermi function becomes $n_F(z_3) = n_F(i\Omega_n - E) = n_F(-E)$. The last step is crucial. Had we not replaced eV by $i\Omega_n$, we would have gotten $n_F(eV - E)$ which is the wrong distribution and will give a thermal smearing for eV near the gap Δ.

After this step we can set $i\Omega_n \to eV - i\eta$. A pole appears at $E = eV + i\eta$. Taking the imaginary part of $J_i(i\Omega_n \to eV + i\eta)$ gives a delta function $\delta(2eV - 2E)$. This is the expression of energy conservation: the tunneling of a Cooper pair gains an energy $2eV$ which are used to excite two quasiparticles each at energy E. This is because momentum is conserved on average after averaging over the random tunneling amplitudes and a pair of quasiparticles with opposite

momenta $\boldsymbol{p}$ and $-\boldsymbol{p}$ and equal energy E are created. For $eV > \Delta$ this opens up a new threshold for conduction. The contribution of this diagram is given by

$$I^{\mathrm{MAR}}_{\mathrm{planar},i} = e\frac{\pi^3}{2}|t_0|^4 N_L^2(0)N_R(0)A\frac{eV}{\sqrt{(eV)^2-\Delta^2}} \times [n_F(-eV)-n_F(eV)]. \tag{B4}$$

Inclusion of the other diagrams only changes the numerical prefactor. The important thing to note is that the current appears as an inverse square root divergence above the threshold. This just reflects the density of states of finding the quasiparticle and is very different from the step singularity in the well-known STM case. As we shall see below, this is because in that case a pair of quasiparticles at energy E_p and $E_{p'}$ are excited and a convolution over two quasiparticle density of states appear. Also note that the thermal factor $n_F(-eV)-n_F(eV)$ comes from the poles at z_3 and z_2. This factor equals unity up to corrections of order $e^{-\Delta/T}$ which is negligible. Therefore there is no thermal smearing of the square root divergence near threshold.

It is useful to express the results in terms of the conductance $1/R_N$ of the tunnel junction, which, in the diffusive case, is given by

$$\frac{1}{R_N} = 4\pi\frac{e^2}{\hbar}|t_0|^2 N_L(0)N_R(0)A, \tag{B5}$$

and consider the ratio of the MAR current to the normal-state current at $eV = 2\Delta$, $I_N = \frac{2\Delta}{eR_N}$. We also set $N_R(0) = \frac{m}{2\pi} = \frac{k_F^2}{4\pi E_F}$ where k_F and E_F are the Fermi momentum and Fermi energy of the R SC. We find

$$\frac{I^{\mathrm{MAR}}_{\mathrm{planar}}}{I_N} \propto \frac{g}{Ak_F^2}\frac{E_F}{\Delta}\frac{eV}{\sqrt{(eV)^2-\Delta^2}}. \tag{B6}$$

We can interpret Ak_F as the number of tunneling channels and $\mathcal{T}_{\mathrm{eff}} = \frac{g}{Ak_F^2}$ as the tunneling probability per channel. $\mathcal{T}_{\mathrm{eff}}$ describes the intrinsic transparency of a planar junction.

We can repeat the calculation for the smooth planar junction where momentum parallel to the interface is conserved. A representative diagram is shown in Fig. 4(b). Now there is only a single momentum sum and the results when expressed in terms of the conductance are essentially the same as Eq. (B6).

2. MAR: STM junction

We have also reproduced the result for the STM case. A representative diagram is shown in Fig. 4(c). Now there are two momentum sums over $\boldsymbol{p}$ and $\boldsymbol{p}'$, resulting in two energy integrals. Taking the imaginary part results in a delta function $\delta(E+E'=2eV)$. This expresses the fact that the energy gained by tunneling a pair is used to excite a pair of quasiparticles with momenta $\boldsymbol{p}$ and $\boldsymbol{p}'$ and energy E and E'. Summing over all diagrams and taking $\Delta_L = \Delta_R = \Delta$, we find for $eV > \Delta$

$$I^{\mathrm{MAR}}_{\mathrm{STM}} = 2e\pi^3|\tilde{t}|^4 N_L^2(0)N_R^2(0)\Delta^2\int_{\Delta}^{2eV-\Delta} \times dE\,\frac{n_F(-E)-n_F(E)}{\sqrt{E^2-\Delta^2}\sqrt{(2eV-E)^2-\Delta^2}}, \tag{B7}$$

leading to a step function at $eV = \Delta$. This agrees with and extends Ref. [14] to finite temperature, demonstrating that the finite-temperature correction is exponentially small in Δ/T. Its ratio to the corresponding normal current I_N is given by

$$\frac{I^{\mathrm{MAR}}_{\mathrm{STM}}}{I_N} = \frac{\pi}{16}g\,\theta(eV-\Delta). \tag{B8}$$

Note that unlike the planar case, the factor $N_R(0)$ in the denominator, which led to the Fermi energy E_F appearing in the numerator of Eq. (B6), does not arise.

We emphasize that there is no thermal smearing of the MAR peak until a temperature comparable to the energy gap Δ is reached. On the other hand, thermal noise gives rise to voltage fluctuations as discussed in the main text. The MAR structure can also be viewed as linear response to the order parameter in the R SC except that quasiparticles are excited instead of a collective mode. Therefore the voltage fluctuation will broaden the MAR structure in the same way as the collective mode is broadened. Thus the minimum broadening is given by Γ_0. In practice, in planar junctions there are other sources of broadening such as local inhomogeneity. The latter is particularly important for many strongly correlated SCs such as cuprates and iron-based SCs.

[1] G. Blumberg, A. Mialitsin, B. S. Dennis, M. V. Klein, N. D. Zhigadlo, and J. Karpinski, Observation of Leggett's collective mode in a multiband MgB_2 superconductor, Phys. Rev. Lett. **99**, 227002 (2007).

[2] J. Paglione and R. L. Greene, High-temperature superconductivity in iron-based materials, Nat. Phys. **6**, 645 (2010).

[3] N. R. Poniatowski, J. B. Curtis, A. Yacoby, and P. Narang, Spectroscopic signatures of time-reversal symmetry breaking superconductivity, Commun. Phys. **5**, 44 (2022).

[4] A. Leggett, Number-phase fluctuations in two-band superconductors, Prog. Theor. Phys. **36**, 901 (1966).

[5] P. Wölfle, Order-parameter collective modes in ^{3}He-*A*, Phys. Rev. Lett. **37**, 1279 (1976).

[6] G. Volovik and M. Zubkov, Higgs bosons in particle physics and in condensed matter, J. Low Temp. Phys. **175**, 486 (2014).

[7] K. Katsumi, Z. Z. Li, H. Raffy, Y. Gallais, and R. Shimano, Superconducting fluctuations probed by the Higgs mode in $Bi_2Sr_2CaCu_2O_{8+x}$ thin films, Phys. Rev. B **102**, 054510 (2020).

[8] R. A. Ferrell, Fluctuations and the superconducting phase transition: II. Onset of Josephson tunneling and paraconductivity of a junction, J. Low Temp. Phys. **1**, 423 (1969).

[9] D. J. Scalapino, Pair tunneling as a probe of fluctuations in superconductors, Phys. Rev. Lett. **24**, 1052 (1970).

[10] V. Ambegaokar and A. Baratoff, Tunneling between superconductors, Phys. Rev. Lett. **10**, 486 (1963).

[11] J. Anderson and A. M. Goldman, Experimental determination of the pair susceptibility of a superconductor, Phys. Rev. Lett. **25**, 743 (1970).

[12] D. Pekker and C. M. Varma, Amplitude/Higgs modes in condensed matter physics, Annu. Rev. Condens. Matter Phys. **6**, 269 (2015).

[13] M. Ternes, W.-D. Schneider, J.-C. Cuevas, C. P. Lutz, C. F. Hirjibehedin, and A. J. Heinrich, Subgap structure in asymmetric superconducting tunnel junctions, Phys. Rev. B **74**, 132501 (2006).

[14] J. C. Cuevas, A. Martín-Rodero, and A. Levy Yeyati, Hamiltonian approach to the transport properties of superconducting quantum point contacts, Phys. Rev. B **54**, 7366 (1996).

[15] O. Naaman and R. Dynes, Subharmonic gap structure in superconducting scanning tunneling microscope junctions, Solid State Commun. **129**, 299 (2004).

[16] A. Steinbach, P. Joyez, A. Cottet, D. Esteve, M. H. Devoret, M. E. Huber, and J. M. Martinis, Direct measurement of the Josephson supercurrent in an ultrasmall Josephson junction, Phys. Rev. Lett. **87**, 137003 (2001).

[17] S. Zhu, L. Kong, L. Cao, H. Chen, M. Papaj, S. Du, Y. Xing, W. Liu, D. Wang, C. Shen *et al.*, Nearly quantized conductance plateau of vortex zero mode in an iron-based superconductor, Science **367**, 189 (2020).

[18] Y. M. Ivanchenko and L. A. Zil'berman, The Josephson effect in small tunnel contacts, Sov. Phys. JETP **28**, 1272 (1969).

[19] H. Takayama, Superconducting fluctuation effects on the S-I-N junction current, Prog. Theor. Phys. **46**, 1 (1971).

[20] T. Cea and L. Benfatto, Signature of the Leggett mode in the A_{1g} Raman response: From MgB_2 to iron-based superconductors, Phys. Rev. B **94**, 064512 (2016).

[21] H. Shim, K. Yoon, J. S. Moodera, and J. P. Hong, All MgB_2 tunnel junctions with Al_2O_3 or MgO tunnel barriers, Appl. Phys. Lett. **90**, 212509 (2007).

[22] W. Wan, P. Dreher, D. Muñoz-Segovia, R. Harsh, H. Guo, A. J. Martínez-Galera, F. Guinea, F. de Juan, and M. M. Ugeda, Observation of superconducting collective modes from competing pairing instabilities in single-layer $NbSe_2$, Adv. Mater. **34**, 2206078 (2022).

[23] V. Grinenko, R. Sarkar, K. Kihou, C. Lee, I. Morozov, S. Aswartham, B. Büchner, P. Chekhonin, W. Skrotzki, K. Nenkov *et al.*, Superconductivity with broken time-reversal symmetry inside a superconducting *s*-wave state, Nat. Phys. **16**, 789 (2020).

[24] Q. Gu, J. P. Carroll, S. Wang, S. Ran, C. Broyles, H. Siddiquee, N. P. Butch, S. R. Saha, J. Paglione, J. Davis *et al.*, Detection of a pair density wave state in UTe_2, Nature (London) **618**, 921 (2023).

[25] G. Koren and P. A. Lee, Observation of two distinct pairs fluctuation lifetimes and supercurrents in the pseudogap regime of cuprate junctions, Phys. Rev. B **94**, 174515 (2016).

[26] M. Hamidian, S. Edkins, S. H. Joo, A. Kostin, H. Eisaki, S. Uchida, M. Lawler, E.-A. Kim, A. Mackenzie, K. Fujita *et al.*, Detection of a Cooper-pair density wave in $Bi_2Sr_2CaCu_2O_{8+x}$, Nature (London) **532**, 343 (2016).

[27] Y. Barlas and C. M. Varma, Amplitude or Higgs modes in *d*-wave superconductors, Phys. Rev. B **87**, 054503 (2013).

[28] J. M. Park, Y. Cao, K. Watanabe, T. Taniguchi, and P. Jarillo-Herrero, Tunable strongly coupled superconductivity in magic-angle twisted trilayer graphene, Nature (London) **590**, 249 (2021).

[29] H. Kim, K. Wang, Y. Nakajima, R. Hu, S. Ziemak, P. Syers, L. Wang, H. Hodovanets, J. D. Denlinger, P. M. Brydon *et al.*, Beyond triplet: Unconventional superconductivity in a spin-3/2 topological semimetal, Sci. Adv. **4**, eaao4513 (2018).

[30] T. Tsuzuki, Effect of thermodynamic fluctuation of the superconductivity order parameter on the tunneling current, Prog. Theor. Phys. **41**, 1600 (1969).